quency source impedance. This limit was effectively reduced by the use of ferrite waveguide components in the radiometer input circuit. A reduction of 98 per cent in the effect of a mismatched radio-frequency source impedance was easily obtained and greater reductions are possible. The input circuit losses introduced by the ferrite components caused a degradation in receiver noise factor of about 10 per cent with a corresponding increase in the minimum detectable power of the system. The use of either a ferrite isolator or a ferrite circulator in the radiometer input circuit will allow accurate measurements of small powers even when some of the critical requirements on the design of the input circuit and antenna are relaxed. In addition, the use of the ferrite circulator as the radiometer comparison switch makes possible a wider variety of direct comparison measurements of microwave noise powers.

ACKNOWLEDGMENT

The author wishes to thank Mr. F. T. Haddock and Drs. W. R. Ferris and J. P. Hagen for many helpful suggestions.

The Characteristic Impedance of the Shielded Slab Line

R. H. T. BATES†

Summary—**The characteristic impedance of the shielded slab line is worked out exactly in terms of elliptic functions. A design graph is given to cover most practical applications.**

LIST OF SYMBOLS

THE NOTATION used for the elliptic functions follows E. T. Copson [1].

z, p, q, s, u, v	Independent complex variables.
a, b, d, t, w	Variable parameters.
$\wp(z)$	Weierstrasse's second order elliptic function.
sn z, cn, z, dn z	Jacobian elliptic functions.
k	Modulus of the elliptic functions.
K	Real quarter period of sn z.
jK'	Imaginary half period of sn z.
$\Theta(z)$	Jacobian theta function.
$Z(z)$	Jacobian zeta function.
ϵ_r	Relative permittivity of medium between shielding plates.

INTRODUCTION

The shielded slab transmission line has several advantages over the coaxial line, especially when it is used as a slotted-line standing wave indicator for wavelengths greater than one foot. The mechanical tolerances are less stringent for a given reading accuracy. A good account of the advantages and disadvantages of this type of standing wave indicator is given by Wholey and Eldred [2], who give design curves for a circular inner conductor.

In a recent paper Cohn [3] has given values of the characteristic impedance of the slab line, calculated from approximate formulas, for t/b less than 0.25, see Fig. 1. However, it is possible to solve the problem exactly, using elliptic functions. As these functions have been comprehensively tabulated, the labor involved in producing the design graphs is probably less than that necessary for evaluating the approximate expressions. Also, the exact formulas allow one to design lines having values of t/b up to unity.

This paper describes the conformal transformations whereby the characteristic impedance of the slab line is determined. The results are shown on a chart, with $\sqrt{\epsilon_r}Zo$ as parameter.

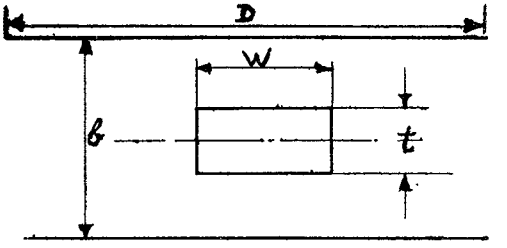

Fig. 1—Geometry of shielded slab line.

EFFECT OF FINITE WIDTH OF SHIELDING PLATES

The characteristic impedance of the slab line from now on will be referred to as Zo.

In the calculation of Zo, the width, D, of the shielding plates is assumed infinite; see Fig. 1. In practice D does not have to be excessively large for this assumption to be valid. There is a convenient method of judging the effect of the finite value of D. The infinite plates are transformed into a cylinder. Then the angular width, θ radians, of the slot in the cylinder due to the finite width of the shielding plates is given by,

$$\theta = 4 \operatorname{cosech} \frac{\pi D}{b}$$

In Fig. 2, θ in degrees is plotted against D/b. It is that the effect of a finite D can easily be made negligible.

† Decca Radar Ltd., Tolworth, Surrey, Eng.

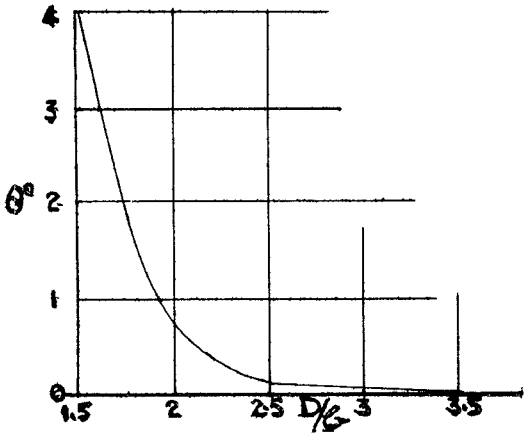

Fig. 2—Angular width of slot in equivalent circular cylinder.

Determination of Z_o

It is convenient to bisect the slab line along that axis of symmetry parallel to the shielding plates. Fig. 3 shows the transformations necessary to change the bisected system into two infinitesimally thin coplanar sheets, one finite and one infinite.

Fig. 4 shows how a system of two coaxial cylinders can be transformed into a parallel plate line [4], exactly equivalent to the one shown in the s plane in Fig. 3. The details of the transformation are shown in Fig. 4. The numerical evaluation is simple for,

$$\frac{\omega_1}{\omega_3} = \frac{K}{jK'}$$

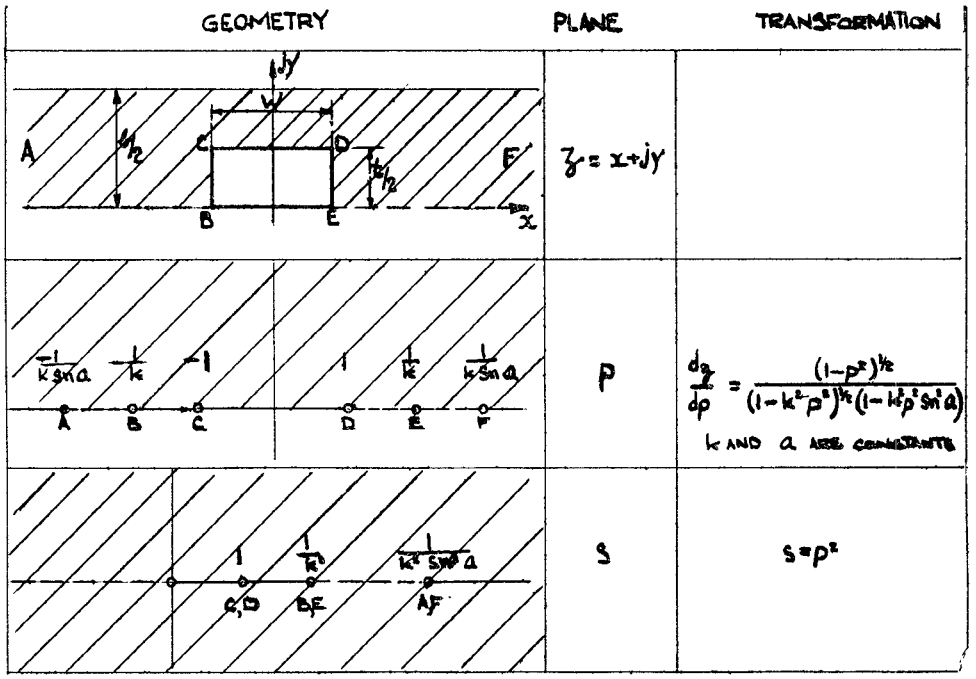

Fig. 3—Full lines represent constant potential boundaries; *i.e.*, conductors. Dotted lines represent streamlines of electric force. Hatching represents the region originally within the slab line after it has been transformed from plane to plane.

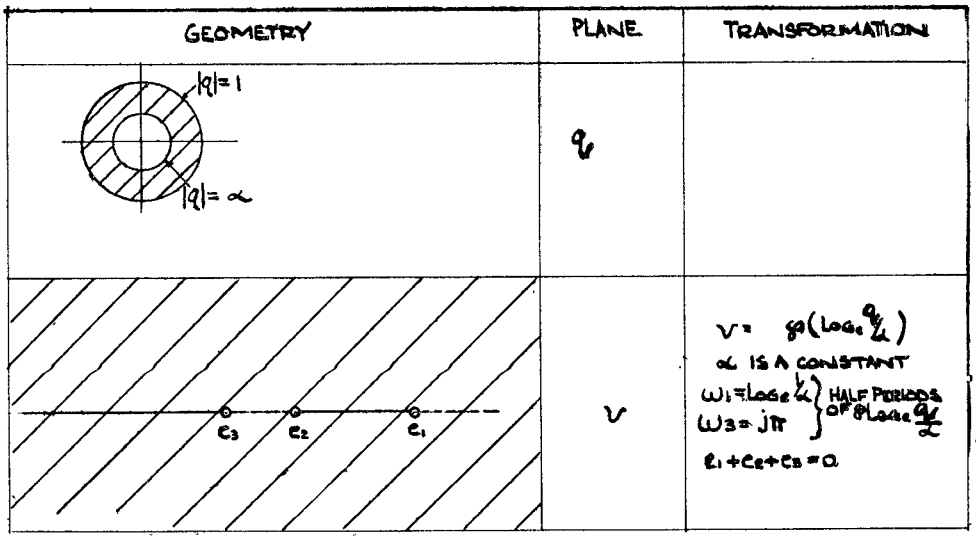

Fig. 4—Transformation of coaxial line into parallel plate line.

and $\omega_1 = \log_e (1/\alpha) = (1/60) \times$characteristic impedance of coaxial cylinders. K and jK' are complete elliptic integrals of the first kind as well as the real quarter period and imaginary half period of sn (z, k).

Only half the original system has been considered, so the characteristic impedance of the coaxial cylinders will be $2Zo$. Fig. 5 (opposite) is a plot of Zo vs $(e_2-e_3)/(e_1-e_3)$. With reference to Fig. 3 it is clear that

$$\frac{e_2 - e_3}{e_1 - e_3} = \mathrm{cn}^2\, a \tag{1}$$

The main part of the problem is the solving of the integral equation derived from the Schwarz-Christoffel transformation from z plane to the p plane, Fig. 3.

$$\int_0^z dz = \int_0^p \frac{(1 - p^2)^{1/2} dp}{(1 - k^2p^2)^{1/2}(1 - k^2p^2\mathrm{sn}^2\, a)} + M$$

where a and M are constants for one set of values of W, t, and b.

Make the substitution,

$$p = \mathrm{sn}\, u \tag{2}$$

Then,

$$z = \int_0^u \frac{(1 - \mathrm{sn}^2\, u)du}{1 - k^2\mathrm{sn}^2\, u\, \mathrm{sn}^2\, a} + M.$$

Refer to the chapter on Jacobian elliptic functions [1]. Transform the above integral into two Legendre elliptic integrals of the first and third kinds respectively. After a little manipulation the above equation reduces to,

$$z = u\left[1 - \frac{\mathrm{dn}\, a\, Z(a)}{k^2\, \mathrm{sn}\, a\, \mathrm{cn}\, a}\right] - \frac{\mathrm{dn}\, a}{2k^2\, \mathrm{sn}\, a\, \mathrm{cn}\, a} \cdot \log_e\left[\frac{\Theta(u - a)}{\Theta(u + a)}\right] + M. \tag{3}$$

Now sn a is always less than unity, so a is real. Since $\Theta(z)$ is an even function of z,

$$\frac{\Theta(-a)}{\Theta(a)} = 1.$$

So $z = M$ when $u = 0$. By inspection of Fig. 3 it can be seen that,

$$z = j\frac{t}{2} \quad \text{when} \quad p = 0.$$

From (2), $u = 0$ when $p = 0$. So,

$$M = j\frac{t}{2} \tag{4}$$

Also, $z = W/2$ when $p = 1/k$, $u = K + jK'$. Substituting into (3), using (4), and separating real and imaginary parts,

$$W = 2K\left[1 - \frac{\mathrm{dn}\, a(Z)a}{k^2\, \mathrm{sn}\, a\, \mathrm{cn}\, a}\right] \tag{5}$$

$$t = \frac{\pi\, \mathrm{dn}\, a}{k^2\, \mathrm{sn}\, a\, \mathrm{cn}\, a} \cdot \frac{a}{K} - 2K'\left[1 - \frac{\mathrm{dn}\, aZ(a)}{k^2\, \mathrm{sn}\, a\, \mathrm{cn}\, a}\right] \tag{6}$$

since,

$$\frac{\Theta(K + jK - a)}{\Theta(K + jK + a)} = e^{j\pi a/k}.$$

The constant b is found very simply by integrating along a small semi-circle in the upper half of the p plane about the point $1/k$ sn a, and equating the result to the equivalent change in the z plane. Since the residue at $p = 1/k$ sn a is

$$\frac{\mathrm{dn}\, a}{2k^2\, \mathrm{sn}\, a\, \mathrm{cn}\, a}$$

then,

$$b = \frac{\pi\, \mathrm{dn}\, a}{k^2\, \mathrm{sn}\, a\, \mathrm{cn}\, a}. \tag{7}$$

Numerical Evaluation of Zo

From (5), (6), and (7), the following normalized expressions can be formed,

$$\frac{W}{b} = \frac{2K}{\pi}\left[\frac{k^2\, \mathrm{sn}\, a\, \mathrm{cn}\, a}{\mathrm{dn}\, a} - Z(a)\right] \tag{8}$$

$$\frac{t}{b} = \frac{a}{K} - \frac{2K'}{\pi}\left[\frac{k^2\, \mathrm{sn}\, a\, \mathrm{cn}\, a}{\mathrm{dn}\, a} - Z(a)\right]. \tag{9}$$

The most convenient way of evaluating these formulas was found to be the following,

a) Take a given value of Zo.
b) From Fig. 5, see (1), find the corresponding value of cn a.
c) Substitute this value of cn a into (8) and (9) and calculate W/b and t/b for several values of k.

Sufficient tables for the calculations were found in Milne-Thomson [5, 6] and Jahnke and Emde. [7]

Fig. 6, on page 32, is a plot of the results of the calculations. $\sqrt{\epsilon_r}Zo$ is the parameter. The graph should cover the design of the majority of slab lines.

Conclusions

The tables of elliptic functions available to the author were not suitable for calculating values of $\sqrt{\epsilon_r}Zo$ less than about 30Ω and greater than about 200Ω. However, approximate formulas can give accurate answers for values of $\sqrt{\epsilon_r}Zo$ less than about 30Ω. The approximate formulas used by the author were similar to those used by Cohn and have therefore not been described.

The results given by Cohn [3] agree well with those of this paper, which shows that approximate expressions give good answers for small values of t/b. It appears, however, that the exact formulas, (8) and (9), are needed for calculating $\sqrt{\epsilon_r}Zo$ for values of t/b greater than about 0.25 and for values of w/b less than about 0 1.

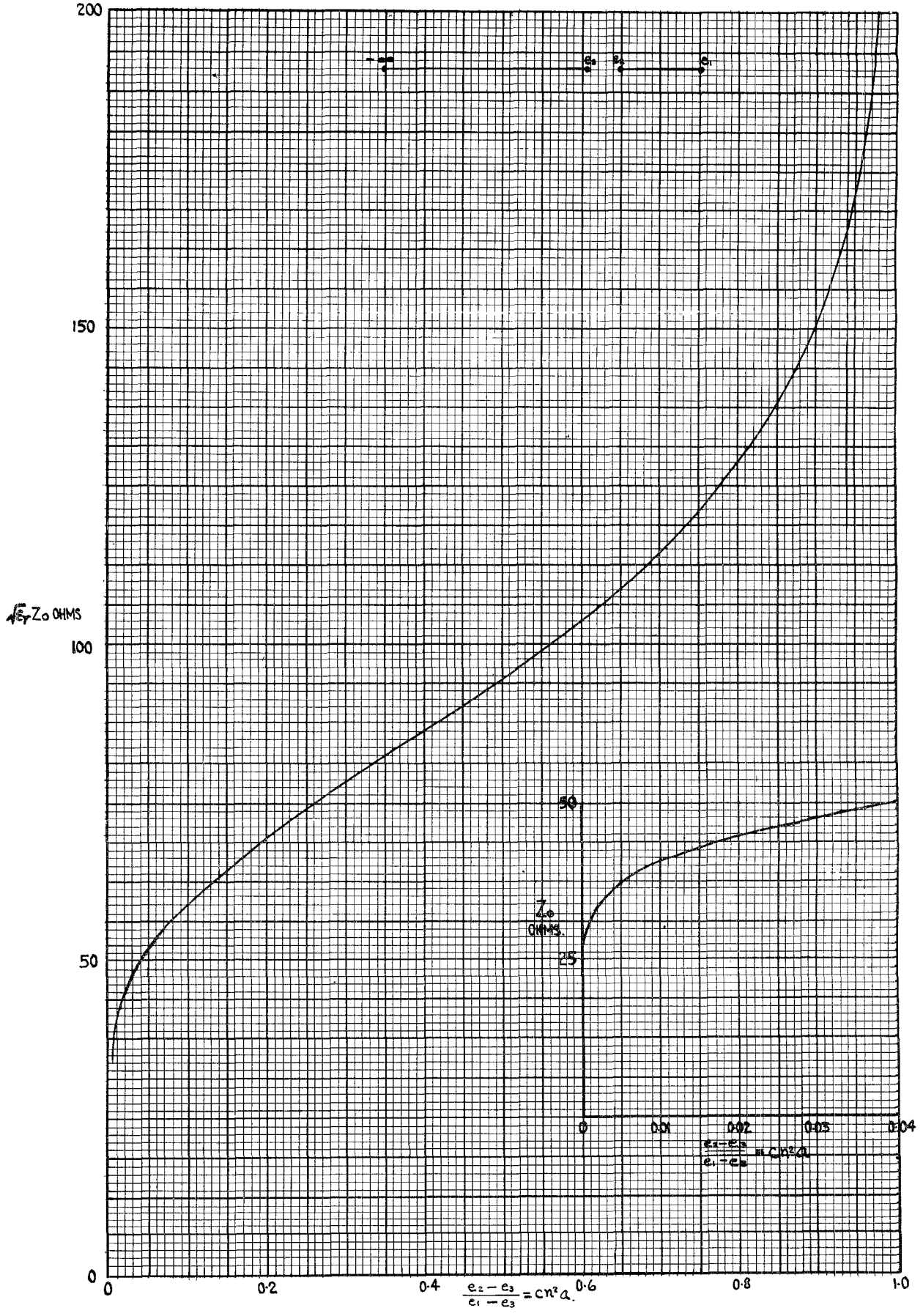

Fig. 5—*Zo* versus $cn^2\,a$.

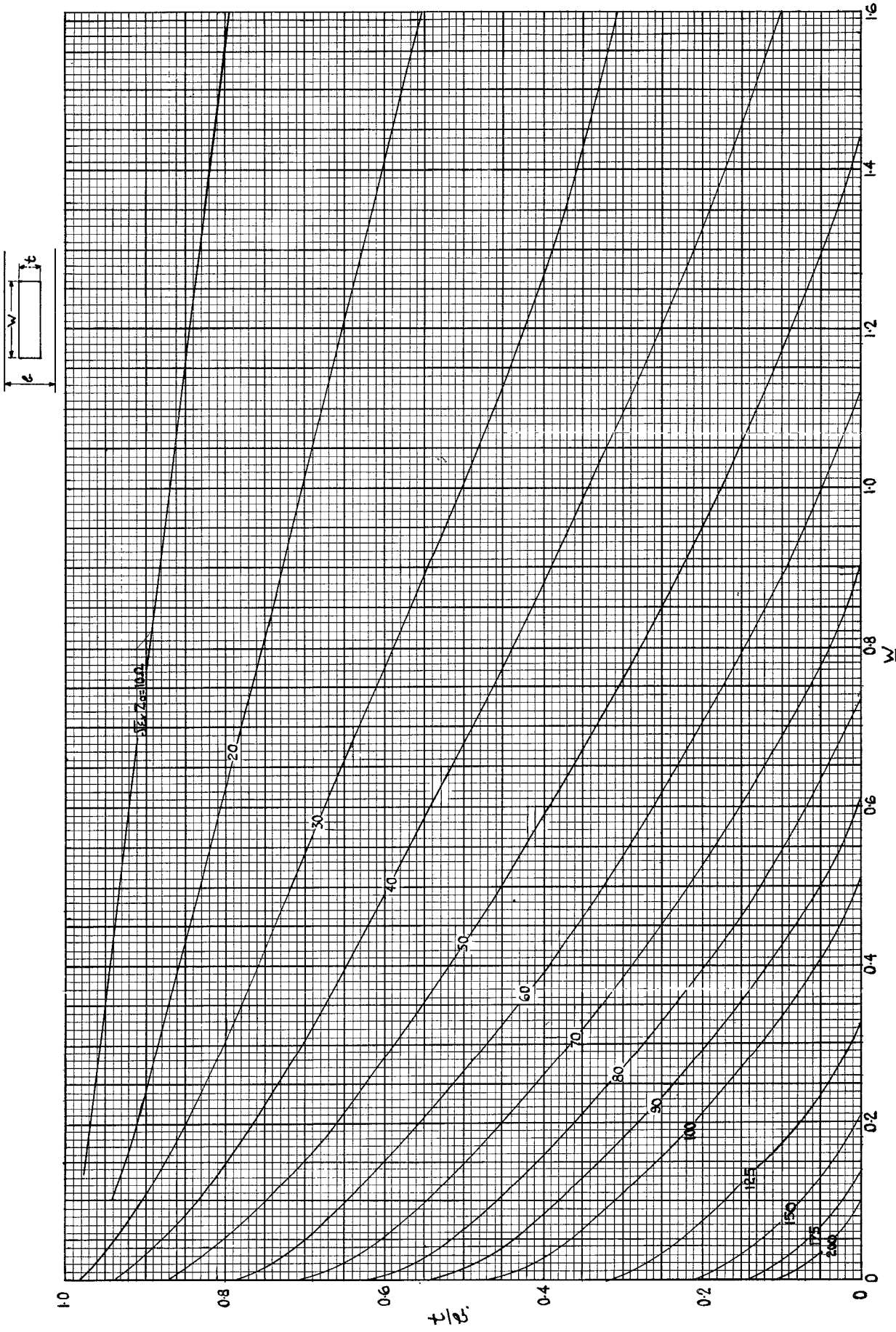

Fig. 6—t/b vs w/b with $\sqrt{\epsilon_r}Z_0\Omega$ as parameter.

ACKNOWLEDGMENT

The permission of Vickers-Armstrongs Ltd. to publish this note is gratefully acknowledged.

BIBLIOGRAPHY

[1] Copson, E. T., *Functions of a Complex Variable*. Oxon. University Press. London, 1950.
[2] Wholey, W. B., and W. N. Eldred, "A New Type of Slotted Line Section." *Proceedings of the IRE*, Vol. 38, (March, 1950), pp. 244–248.
[3] Cohn, S. B., "Characteristic Impedance of the Shielded-Strip Transmission Line," *Transactions of the IRE* (PGMTT), Vol. MTT-2, (July, 1954), pp. 52–57.
[4] Kober, H., *Dictionary of Conformal Representation*, New York, Dover Press. New York, 1952.
[5] Milne-Thomson, L. M., *Die Elliptischen Funktionen von Jacobi*. Berlin, Springer, 0000.
[6] Milne-Thomson, L. M., "The Zeta Function of Jacobi." *Proceedings of the Royal Society of Edinburgh*, Vol. 52, Part II, No. 11 (1931, 1932).
[7] Jahnke, E., and F. Emde, *Funktionentafeln*. Leipzig & Berlin, Teubner.

Characteristics of a New Serrated Choke

KIYO TOMIYASU† AND J. J. BOLUS‡

Summary—**A new type of serrated choke will permit cuts or gaps anywhere on the walls of a rectangular waveguide. The low gap impedance is provided essentially by closely spaced, quarter-wavelength, open-ended, two-wire-line stubs. Low power and high power characteristics of many designs are presented.**

INTRODUCTION

A NEW choke has been designed and tested which will permit cuts, slots, or gaps on waveguide walls hitherto considered impossible. Previously, only slots on the center of the broad wall of a guide supporting the dominant TE_{10} mode as well as gaps in a transverse plane, such as a choke flange, were permitted. However, with the new serrated choke, slots or gaps are permitted anywhere on the guide walls; *e.g.*, on the narrow wall in the longitudinal direction, on the broad wall not at its center, cuts or gaps at any angle on any wall, etc. Applications of the new choke are possible in microwave components and scanning antennas.

Essentially the required low impedance across a gap is provided by closely spaced quarter-wavelength open-ended two-wire line stubs. A schematic diagram of a longitudinal serrated choke is shown in Fig. 1(a). The second conductors of the two-wire line stubs are provided by the images of the serrations as shown in Fig. 1(b) and Fig. 1(c).

It may appear feasible to design a longitudinal choke without the serrations. Such a choke was actually tried but without success. A section of a waveguide 12 inches long with unserrated choke was connected into a $1 \times \frac{1}{2}$ inch rectangular waveguide measuring setup. The input vswr varied from 1.05 to 3 and the insertion loss varied from 0.5 to 3 db as the effective length of the unserrated choke was varied using an adjustable short. The large variation in characteristics is due to the coexistence of two propagating waveguide modes in the choked waveguide region. These two modes could be considered as the $TE_{1/2,0}$ and $TE_{3/2,0}$ modes relative to the choked waveguide. The latter mode yields the dominant TE_{10} mode in unchoked rectangular waveguide. Inasmuch as these two modes have different cutoff wavelengths, whose ratio may be about 4, the respective propagation velocities will differ. This will result in a spatial beating and hence partial power transfer characteristics between the primary waveguide and the "choke" waveguide.[1] By serrating the choke, the $TE_{1/2,0}$ mode will not propagate and the desired low impedance will be provided across the gap.

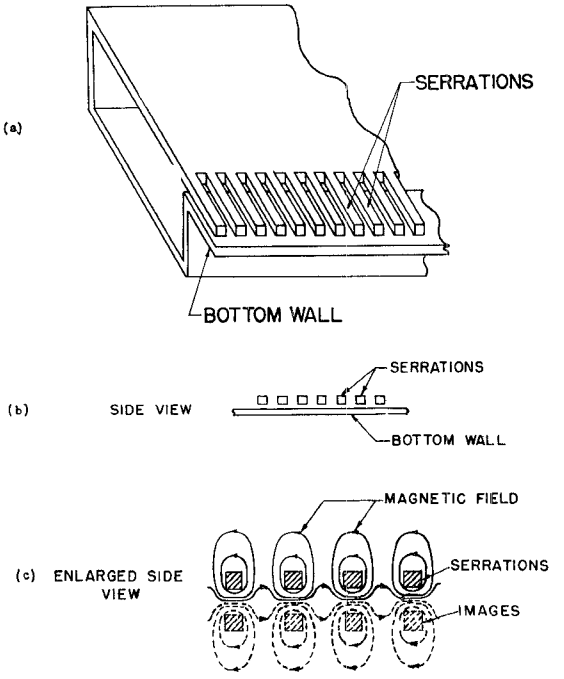

Fig. 1—The serrated choke.

† Formerly with Sperry Gyroscope Co., Great Neck, N. Y., now with Gen. Elec. Microwave Lab., Palo Alto, Calif.

‡ On leave from Sperry Gyroscope Co., now at Signal Corp Engrg. Labs., Ft. Monmouth, N. J.

[1] K. Tomiyasu and S. B. Cohn, "The transvar directional coupler," PROC. IRE, vol. 41, pp. 922–926; July, 1953.